Carbon-based polymer dots sensor for breast cancer detection using peripheral blood immunocytes

Meng-Xian Liu,[a,‡] Shuai Chen,[b,‡] Na Ding,[a] Yong-Liang Yu*[,a] and Jian-Hua Wang*[,a]

[a] *Research Center for Analytical Sciences, Department of Chemistry, College of Sciences, Northeastern University, Box 332, Shenyang 110819, China*

[b] *College of Life and Health Sciences, Northeastern University, Shenyang 110169, China*

[‡] *Both authors have equally contributed to this work.*

Corresponding authors.

*E-mail: yuyl@mail.neu.edu.cn (Y.-L. Yu); jianhuajrz@mail.neu.edu.cn (J.-H. Wang)

Tel: +86 24 83688944; Fax: +86 24 83676698

Electronic Supplementary Information

Chemicals and materials

Hydrogen peroxide (H_2O_2, 30%), sephadex G-25, and n-octanol were purchased from Aladdin Chemistry Co., Ltd. (Shanghai, China). o-phenylenediamine (o-PD), m-phenylenediamine (m-PD), p-phenylenediamine (p-PD), nitric acid (HNO_3), sodium hydroxide (NaOH), sodium chloride (NaCl), potassium chloride (KCl), tetrahydrofuran (THF), sodium phosphate dibasic dodecahydrate ($Na_2HPO_4 \cdot 12H_2O$), potassium phosphate monobasic (KH_2PO_4), and manganese dioxide (MnO_2) were purchased from Sinopharm Chemical Reagent Co., Ltd. (Shanghai, China). Hydrochloric acid (HCl) was purchased from Tianjin Bodi Chemical Co., Ltd. (Tianjin, China). Red blood cell lysis buffer was purchased Solarbio Science and Technology Co., Ltd. (Beijing, China). Streptomycin and penicillin were purchased from Invitrogen (USA). RPMI-1640 media, high glucose medium (DEME), trypsin, and fetal bovine serum (FBS) were purchased from Hyclone (Logan, USA). Unless specified otherwise, all chemicals were of analytical purity grade and used directly without further purification. Deionized water with a resistivity of 18 MΩ·cm was used throughout this study.

Instrumentations

UV/vis absorption spectra were obtained on a U-3900 UV/vis spectrophotometer (Hitachi, Japan). Photoluminescence behavior was obtained on an F-7000 fluorescence spectrophotometer (Hitachi, Japan). Fourier transform infrared (FTIR) spectra were performed on a Nicolet-6700 spectrophotometer (Thermo Instruments Inc., USA). X-ray photoelectron spectroscopy (XPS) scanning curves were obtained on an ESCALAB 250 surface analysis platform (Thermo Electron, USA). Transmission electron microscopy (TEM) images were recorded on a JEM-2100 high resolution transmission electron microscope (JEOL, Japan). The pH values were measured by a PB-10 pH meter (Beijing Sartorius Instruments Co., Ltd., China). Fluorescence lifetime was measured by FluoroMax-4 TCSPC spectrofluorometer (HORIBA Jobin Yvon, USA). The quantum yields (QY) were recorded on a Quantarus-QY absolute photoluminescence quantum yield measurement system (Hamamatsu Photonics, Japan). Cell images were recorded on a FV-1200 confocal laser scanning microscope (Olympus, Japan).

Preparation of CPDs

These CPDs were prepared by oxidative polymerization method. For m-CPDs, 1 mL of concentrated HNO_3 was poured into 400 μL of 0.25 M mPD aqueous solution in one lot. After that 2 mL of H_2O_2 was added, and finally the mixture was diluted to 8 mL with deionized water. The reaction was carried out for 12 h at room temperature. The mixture was adjusted to pH 7 with NaOH solution, followed by removing large particles via filtering with a 0.22-μm filter. The product was collected by separation with a G25 sephadex column and freeze-drying. For o-CPDs and p-CPDs, 2 mL of H_2O_2 was poured into 400 μL of 0.25 M oPD (pPD) aqueous solution, and then the mixture was diluted to 8 mL with deionized water. The reaction was carried out for 12 h at room temperature. Solid products were obtained by the same purification method as described above.

Cell culture

MCF-7, A549, bEnd.3, K562, HepG2, MDA-MB-231, and HeLa cells were all obtained from American Type Culture Collection (ATCC, Manassas, VA). MCF-7, A549, bEnd.3, HepG2, MDA-MB-231, and HeLa cells were cultured in DMEM medium containing 10% (v/v) fetal bovine serum and 1% (v/v) penicillin/streptomycin. K562 were cultured in RPMI-1640 media containing 10% (v/v) FBS and 1% (v/v) penicillin/streptomycin. All cell lines were cultured on 25 cm^2 cell culture plates at 37 °C under a 5% CO_2 humidified atmosphere. The culture medium was changed every day.

Confocal Imaging

MCF-7 cells were seeded onto a glass bottom dish 24 h prior to microscopy measurement. For imaging, the medium was removed and then the attached cells were washed with Opti-MEM (DMEM with 1% (v/v) penicillin/streptomycin). Next, the cells were incubated in Opti-MEM with 200 μg mL^{-1} CPDs for 2 h. Then the living cells were washed with PBS for three times and visualized in PBS.

Animal models

In accordance with the guidelines of the China Animal Care Committee and with the ethical approval from the Animal Care Committee of Northeastern University, mice were fed with standard rat food and raised in a specific pathogen-free barrier facility.

(1) Mouse model of inflammatory disease

Dextran Sulfate Sodium (DSS)-induced ulcerative colitis mice were purchased from Shanghai R&S Biotechnology Co., Ltd. DSS has been widely used to construct colitis model in mice.[1] DSS disrupts the colonic mucosal barrier and leads to colonic inflammation, tissue damage, rectal bleeding and weight loss. The mouse model was constructed as follows: 6-week-old BALB/c mice were fasted but not forbidden to drink water for 24 h before the experiment. Subsequently, the tail of the mouse was lifted and suspended to excrete feces in the distal large intestine. Mice were free to drink 5% DSS solution for 14 days to induce acute colitis.

(2) Mouse models of breast cancer and metastatic breast cancer

Mouse models of breast cancer and metastatic breast cancer were constructed using MCF-7 cells[2] and MDA-MB-231 cells.[3] The 6-week-old female BALB/c nude mice were provided by Beijing HFK Bioscience Co., Ltd. The production license number is SCXK (Beijing) 2019-0088, SPF. The feed for mice was SPF experimental animal feed, and the drinking water was sterilized ultrapure water. The nude mice were acclimated in the animal room (temperature controlled at 24 °C and 12 h light/dark cycles) for one week before the experiment.

After one week adaptive feeding, 200 μL (100 μL Matrigel and 100 μL MCF-7/MDA-MB-231 cells) of cells (2×10^6 cells) were inoculated subcutaneously in the armpit. Continue feeding, MCF-7 mouse models need to be intramuscularly injected

with cycloestradiol propionate (3.0 mg kg^{-1}) once a week, while MDA-MB-231 are ER negative and MDA-MB-231 mouse molels do not need estrogen for growth.[3b] Twice a week, two different dimensions of tumor length were measured by vernier caliper until the tumor volume is approximately 0.5 cm^3. The volume of each tumor was determined by the formula: $V=0.5W^2L$, where V was the tumor volume [cm^3], W was width represent the shorter tumor diameter, and L was long represent the longer tumor diameter.[2c]

Extraction of peripheral blood immunocytes

1 mL of fresh whole blood from healthy, inflammatory, breast cancer, or metastatic breast cancer mice was added to a 15-mL centrifuge tube, followed by the addition of 3 mL of red blood cell lysis buffer. Closed the lid and gently mixed it upside down for several times. After incubating for 5 min at room temperature, the mixture was centrifuged at 2500 rpm for 5 min. The supernatant was removed, and a visible white block appeared at the bottom of the tube. Then the white block was washed with 1 mL of PBS buffer. Finally, peripheral blood immunocytes were obtained by centrifugation at 2500 rpm for 5 min, then dispersed into 1 mL of PBS and counted with microscope on cell counting plate.

Statistical analysis and math models

(1) Linear discriminant analysis (LDA)

For LDA, the raw data matrix was analyzed using IBM SPSS Statistics 22 software. All analytical observations were used in the statistical analysis. The original fluorescence response patterns were converted into standard scores by the description algorithms in IBM SPSS Statistics 22 and all observations were grouped under the condition that the ratio of the inter-class variance to the intra-class variance is maximized according to the pre-assigned group. In blind sample measurement, the fluorescence intensity ratio of an unknown sample was first converted to a standard score. Then the square of the Mahalanobis distance was calculated between the unknown sample and the centroid of the model group. The unknown samples were assigned to the group with the shortest Mahalanobis distance from the model group samples.[4]

The jackknifed classification matrix presents the results of cross-validation (leave-one-out) routine in LDA. The analysis generates a discriminant function by leaving out one channel observations of the set at a time and using the remaining observations as a training set, and then reclassifies the samples to verify the correctness of the system in sample classification. This is performed for each observation, and the overall ability to classify observations represents the quality and predictability of the system.[4]

(2) Hierarchical clustering analysis (HCA)

The raw data matrix was analyzed using IBM SPSS Statistics 22 software for HCA. All analytical observations were used in the statistical analysis. First, the original fluorescence response pattern was converted into a standard score, and the similarity between each class of analytical observations and all analytical observations

was determined by calculating the square of the Euclidean distance between them. The smaller the distance, the higher the similarity, and the two closest data points or categories were combined to generate a clustering tree.[4]

(3) True positive rate (TPR) and False positive rate (FPR)

TPR represents the proportion of real positive samples that currently allocated to positive samples in all positive samples. It was determined by the formula:

$$TPR=TP/(TP+FN)$$

where TP was true positives and FN was false negative.

FPR indicates the proportion of real negative samples that are wrongly classified into positive samples in the total number of all negative samples. It was determined by the formula:

$$FPR=FP/(FP+TN)$$

where FP was false positives and TN was true negatives.[5]

Sensing studies of six cell lines

(1) Detection limit study

50 μL of 20 μg mL^{-1} m-CPDs (o-CPDs and p-CPDs) solution was added to 500-μL centrifuge tube, followed by addition of 50 μL of cell suspension (5×10^4, 2×10^4, 1×10^4, or 5×10^3 cells mL^{-1}) or PBS buffer, and finally the mixture was diluted to 500 μL with PBS. The mixtures were incubated at room temperature (25 °C) for 20 min before the fluorescence intensities were recorded at Ex/Em (nm) 380/463 nm for m-CPDs (370/550 nm for o-CPDs and 470/533 nm for p-CPDs). The fluorescence intensity of the sensor only (without any analytes) is I_0, while the intensity of the sensor with analytes is I. The relative fluorescence intensity of each sample is $(I-I_0)/I_0$. This procedure was repeated to produce four replicates to obtain a training data matrix of 3 signals×6 cell lines× 4 replicates. The data matrix was processed by LDA and/or HCA.

(2) Concentration dependence study

The experimental and data processing were the same as those of the detection limit study except that the analytes were A549 and bEnd.3 cells at six different concentrations (200, 500, 800, 1000, 2000, and 5000 cells mL^{-1}) and the obtained training data matrix was of 3 signals×12 samples×4 replicates.

(3) Discrimination of cells mixture

The experiment and data processing were the same as those of the detection limit study, except that the analytes were mixture of A549 and bEnd.3 cells with a total concentration of 2000 cells mL^{-1} but different proportions (0:10, 1:9, 1:4, 1:1, 4:1, 9:1, and 10:1) and mixture of A549/bEnd.3, A549/HepG2, A549/MCF-7, bEnd.3/HepG2, bEnd.3/MCF-7, and MCF-7/HepG2 cells with a concentration ratio of 1:1 and a total concentration of 2000 cells mL^{-1} and the obtained training data matrixes were of 3

signals×7 samples×4 replicates and 3 signals×6 samples×4 replicates, respectively.

Sensing studies of immunocyte

(1) Detection limit study

50 μL of 20 μg mL^{-1} m-CPDs (o-CPDs and p-CPDs) solution was added to 500-μL centrifuge tube, followed by addition of 50 μL of immunocyte suspension from tumor-free and tumor-bearing (breast cancer) mice (2×10^4 or 1×10^4 cells mL^{-1}) or PBS buffer, and finally the mixture was diluted to 500 μL with PBS. The conditions of incubation and collection of relative fluorescence intensity of each sample were as mentioned above in the part of sensing studies of six cell lines. This procedure was repeated to produce five replicates to obtain a training data matrix of 3 signals×4 samples×5 replicates. The data matrix was processed by LDA and HCA.

(2) Interference study

The experimental and data processing were the same as those of the detection limit study in sensing studies of immunocyte except that the immunocyte samples were from healthy, inflammatory, breast cancer, and metastatic breast cancer mice at the concentration of 2000 cells mL^{-1}.

(3) Individual difference study

The experimental and data processing were the same as those of the detection limit study in sensing studies of immunocyte except that the immunocyte samples were from five normal controls and five breast cancer mice at the concentration of 2000 cells mL^{-1} and the obtained training data matrix was of 3 signals×10 samples×5 replicates.

(4) Blind sample test

For this purpose, we combined data matrix of peripheral blood immunocyte samples from both known (normal and cancerous) and unknown mice models (normal and cancerous) to serve as the reference set. The experimental procedure was the

same as that of the detection limit study in sensing studies of immunocyte except that the immunocyte samples were from known and unknown mice models at the concentration of 2000 cells mL^{-1}. The fluorescence intensity ratio $(I-I_0)/I_0$ of a sample was first converted to a standard score. Then calculate the square of the Mahalanobis distance between the unknown sample and the centroid of the known model group. The unknown samples were assigned to the group with the shortest Mahalanobis distance from the model group samples.

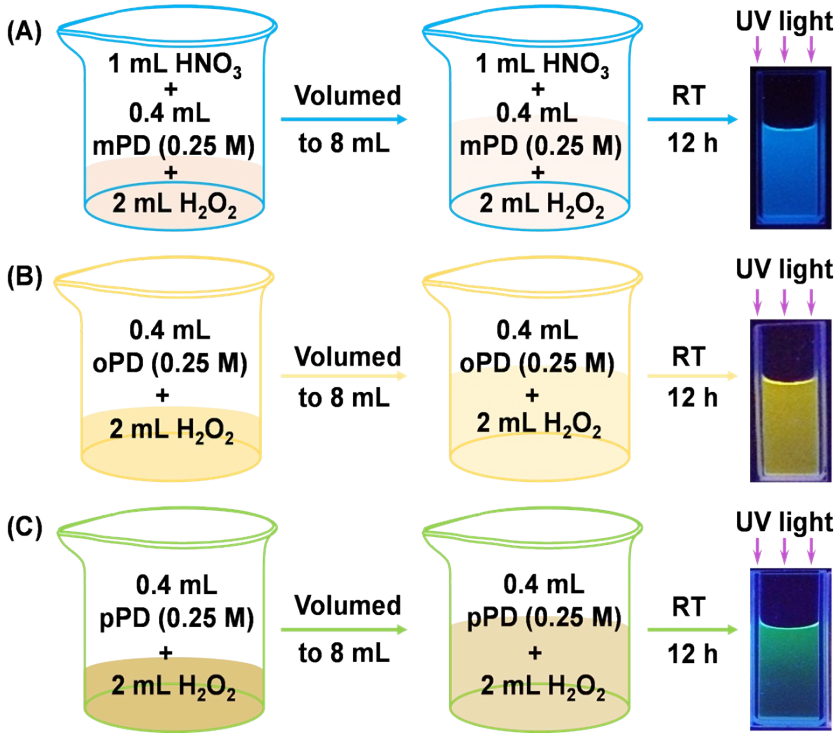

Scheme S1. Preparation of (A) m-CPDs, (B) o-CPDs, and (C) p-CPDs. (Photos of CPDs at 200 μg mL^{-1} under 365 nm UV-light.)

For o-CPDs and p-CPDs, H_2O_2, as a oxidant, can not only introduce oxygen-containing functional groups such as -OH, but also oxidize polymer fragments or monomers into active molecules to condense N-H and C-H bonds to form C-N bonds to expand the conjugation system to form nanometer sized luminescent particles.[6] Due to the relatively weak chemical reactivity of mPD, no luminescent substance is generated when only H_2O_2 is present. Therefore, in this system, HNO_3 not only provides an acidic environment but also acts as an electrophilic addition reagent to introduce nitro into the CPDs structure.[7] In addition, HNO_3 and H_2O_2 can also be used

as oxidants to condense the N-H and C-H bonds between polymer fragments or monomers to form C-N bonds in order to expand the conjugation system.

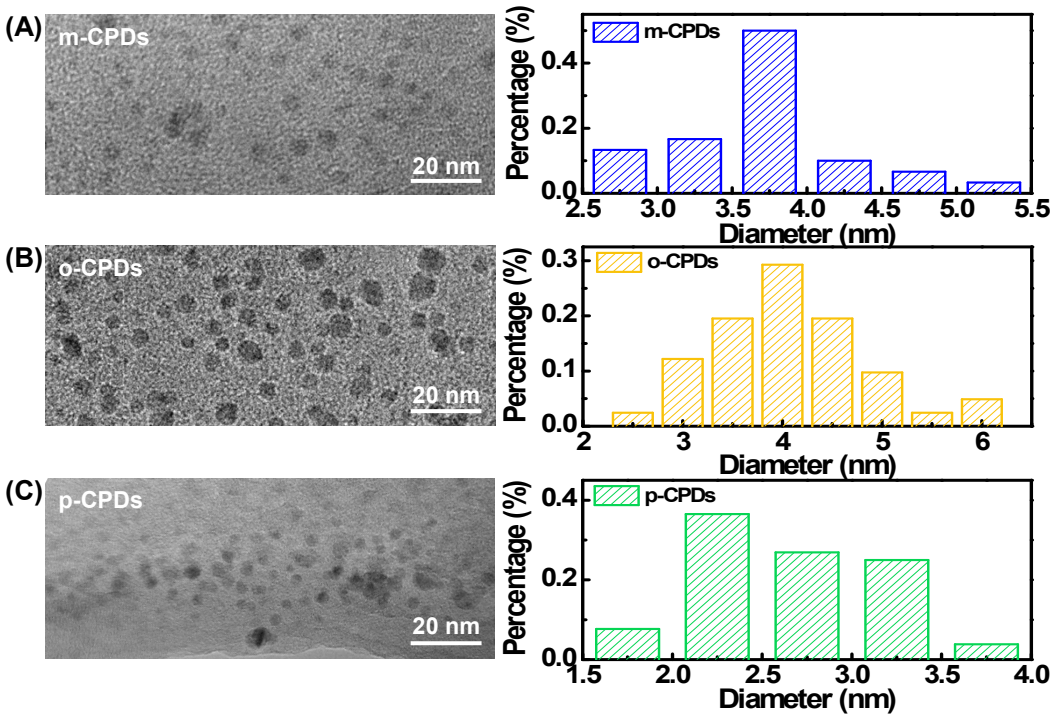

Fig. S1 TEM images and histograms of particles size distribution of (A) m-CPDs, (B) o-CPDs, and (C) p-CPDs.

The results show that these materials are nanoparticles with uniform sizes. The average sizes of m-CPDs, o-CPDs, and p-CPDs are 3.70, 3.80, and 2.65 nm, respectively.

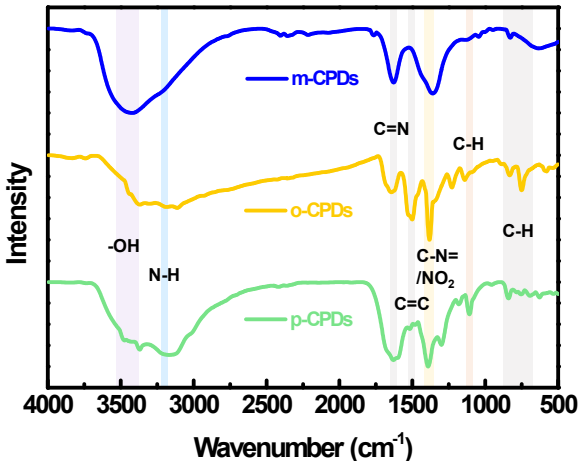

Fig. S2 FTIR spectra of m-CPDs (blue), o-CPDs (orange), and p-CPDs (green).

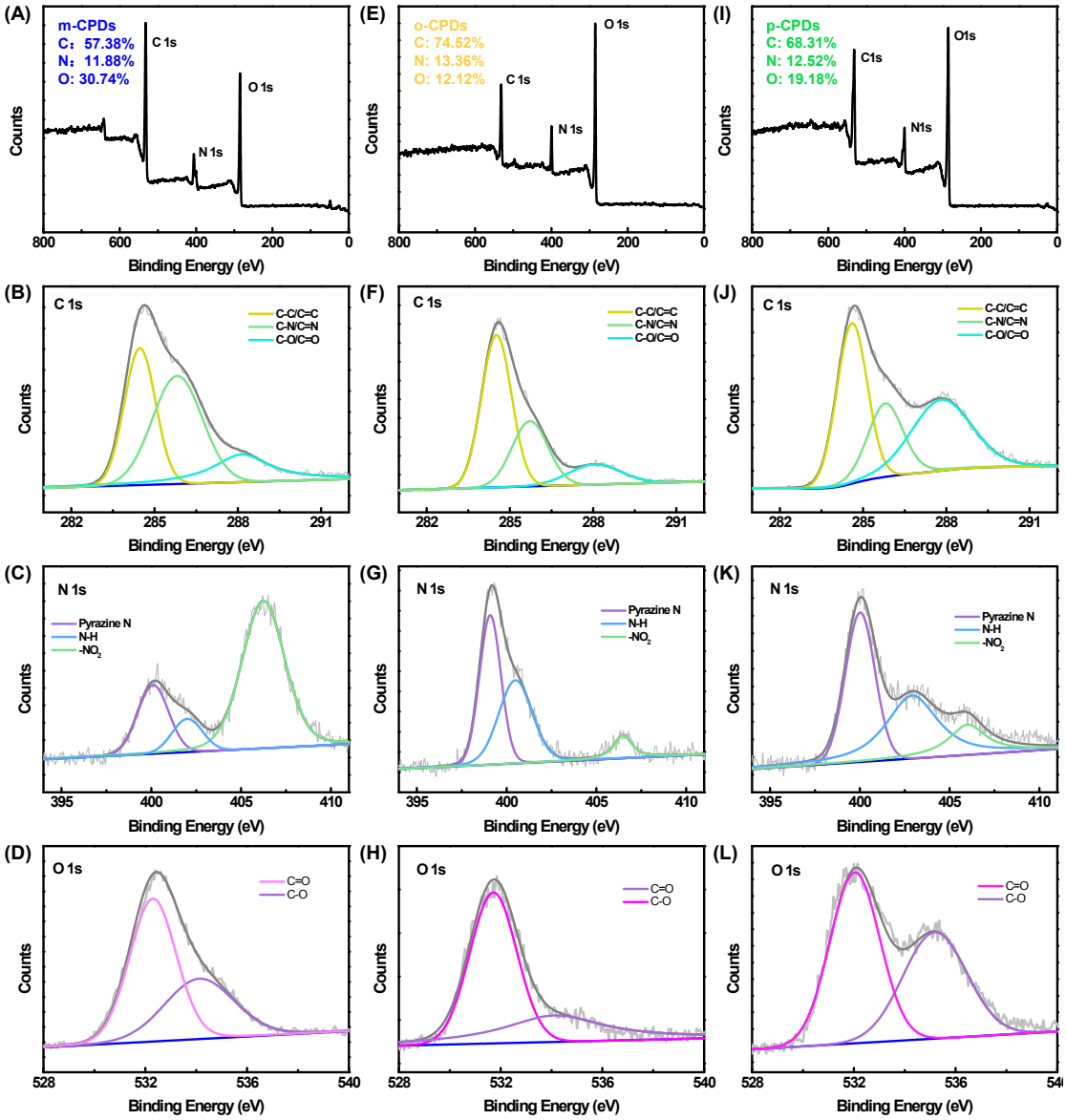

Fig. S3 XPS spectra and deconvoluted high-resolution C 1s, N 1s, and O 1s XPS spectra of m-CPDs (A-D), o-CPDs (E-H), and p-CPDs (I-L), respectively.

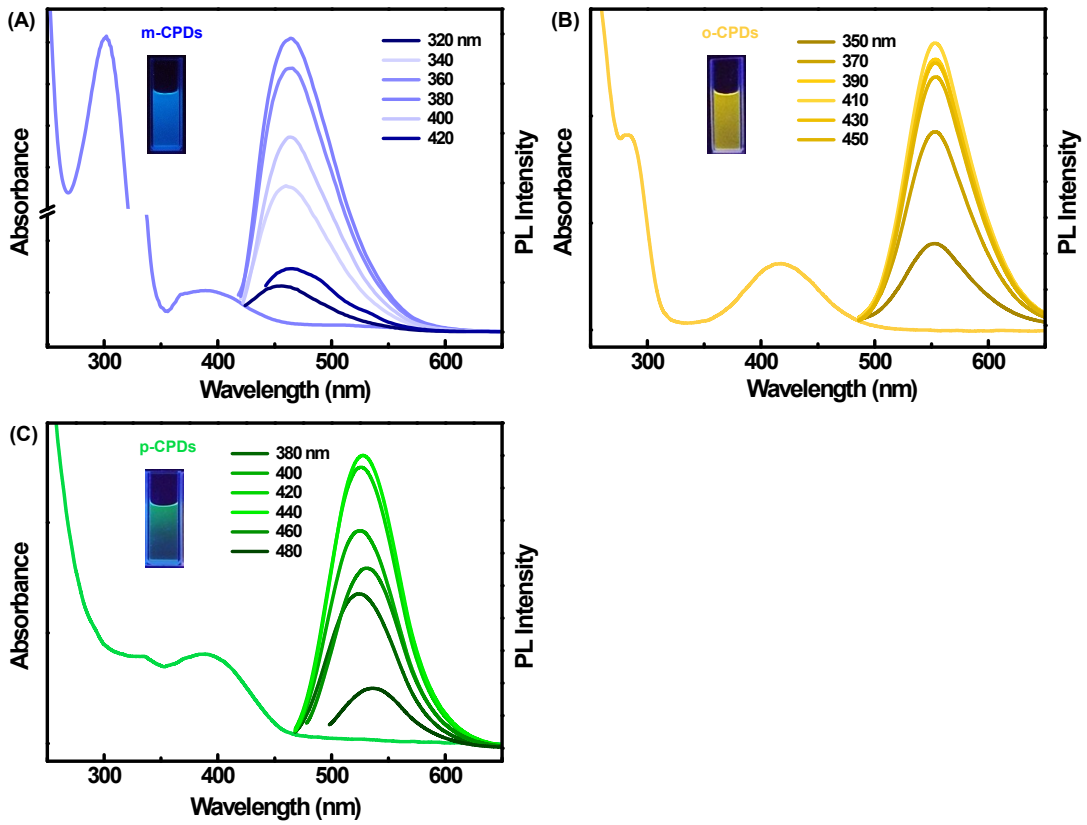

Fig. S4 UV/vis absorption spectra and photoluminescence spectra of (A) m-CPDs, (B) o-CPDs, and (C) p-CPDs (Insets: photos under 365 nm UV-light).

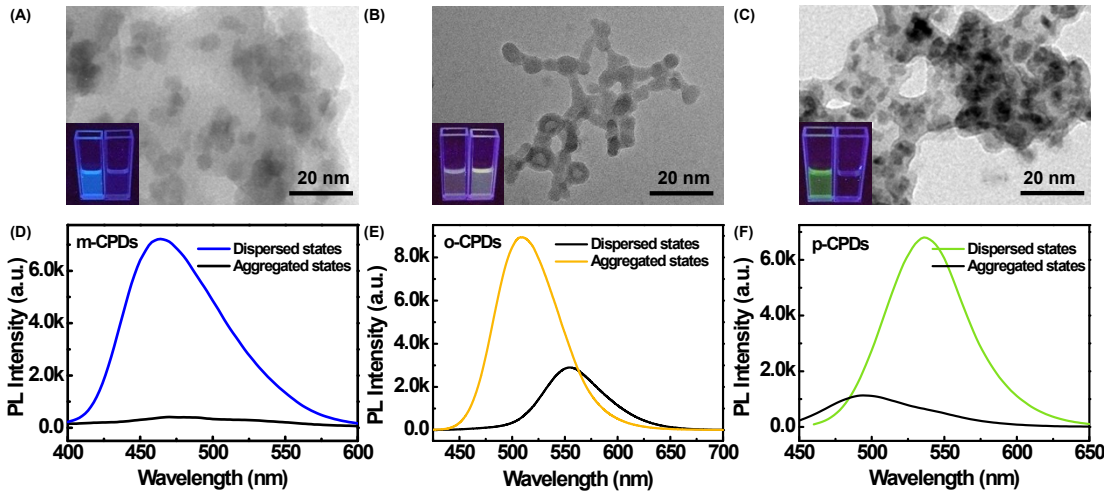

Fig. S5 TEM images and fluorescent spectra of (A and D) m-CPDs, (B and E) o-CPDs, and (C and F) p-CPDs in aggregation state (Insets: photos of CPDs in the dispersed (left) and aggregated (right) states under 365 nm UV-light).

1.00 mg of CPDs (m-CPDs, o-CPDs, and p-CPDs) was weighed and then dispersed into 10 mL of good solvent (water) and poor solvent (THF) to obtain the dispersed state and aggregate state CPDs. TEM images (Fig. S1 and S5) confirmed the formation of dispersed and aggregated states.

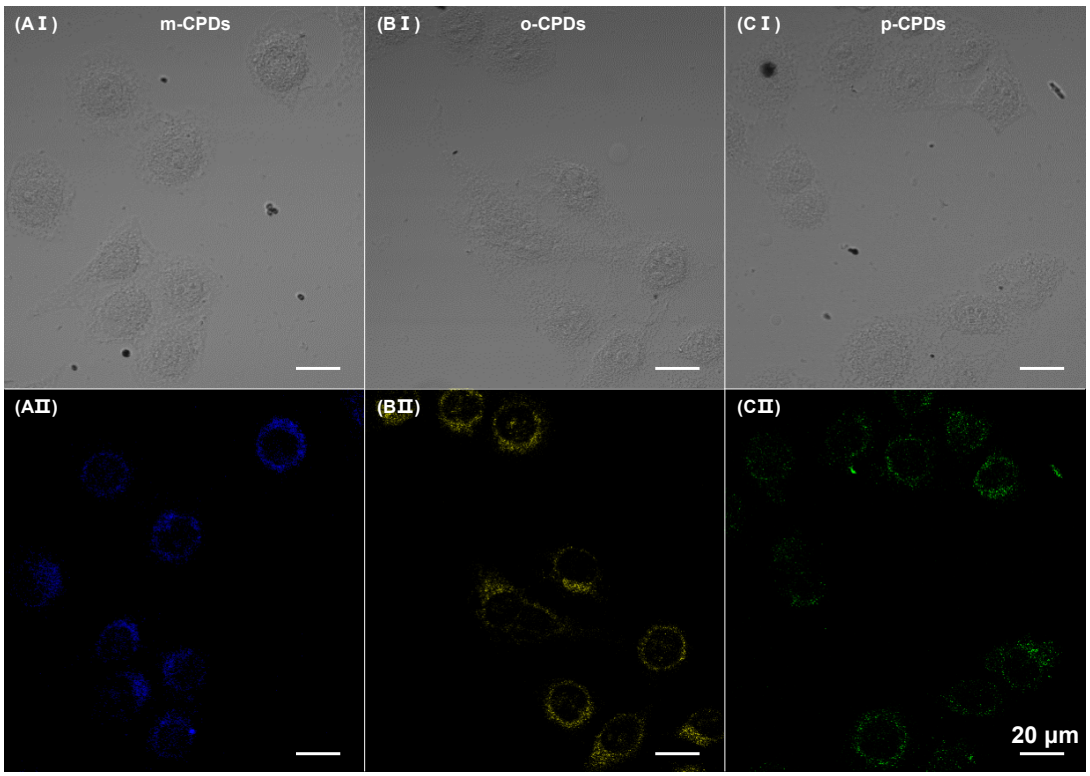

Fig. S6 Confocal laser scanning micrographs (CLSM) showing the binding of CPDs to cell surfaces. Representative images collected in the fluorescence channel and bright field are presented for (A) m-CPDs, (B) o-CPDs, and (C) p-CPDs in combination with MCF-7 cells, respectively. Scale bars: 20 μm.

m-CPDs was excited at 405 nm and the produced emission was collected within 440-480 nm; o-CPDs was excited at 405 nm and the produced emission was collected within 530-570 nm; p-CPDs was excited at 488 nm and the produced emission was collected within 510-550 nm.

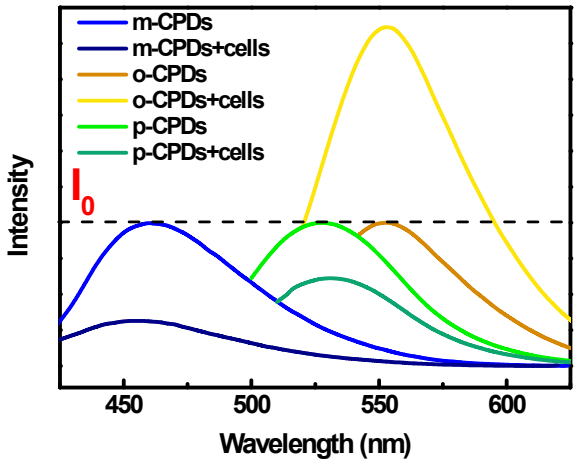

Fig. S7 Photoluminescence spectra of m-CPDs, o-CPDs, and p-CPDs with or without cells.

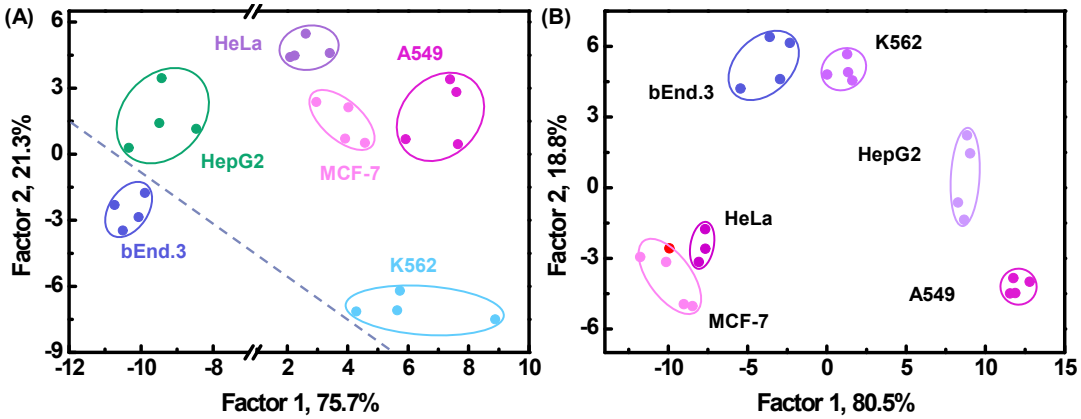

Fig. S8 LDA plot against different cell lines at the concentration of 5000 cells mL^{-1} (A) and 500 cells mL^{-1} (B).

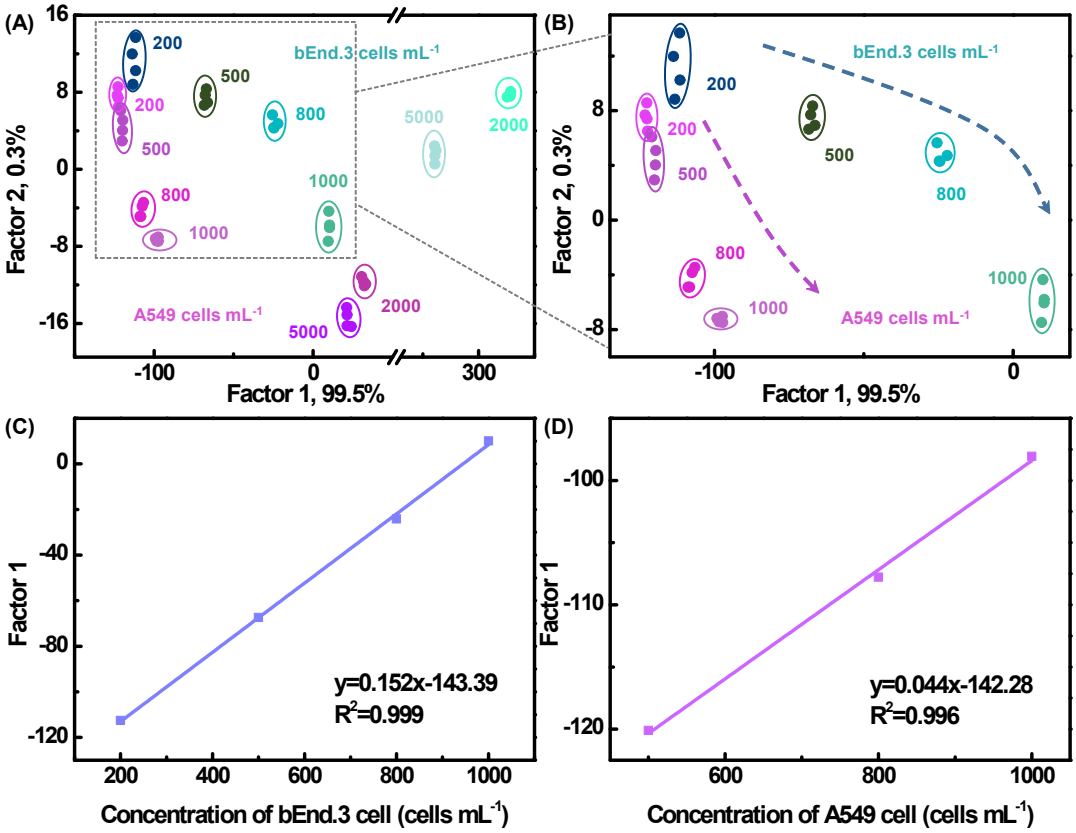

Fig. S9 LDA plot of (A) bEnd.3 and (B) A549 cells against six different concentrations. The linear relationship between the score of Factor 1 and the concentration of (C) bEnd.3 and (D) A549 cells.

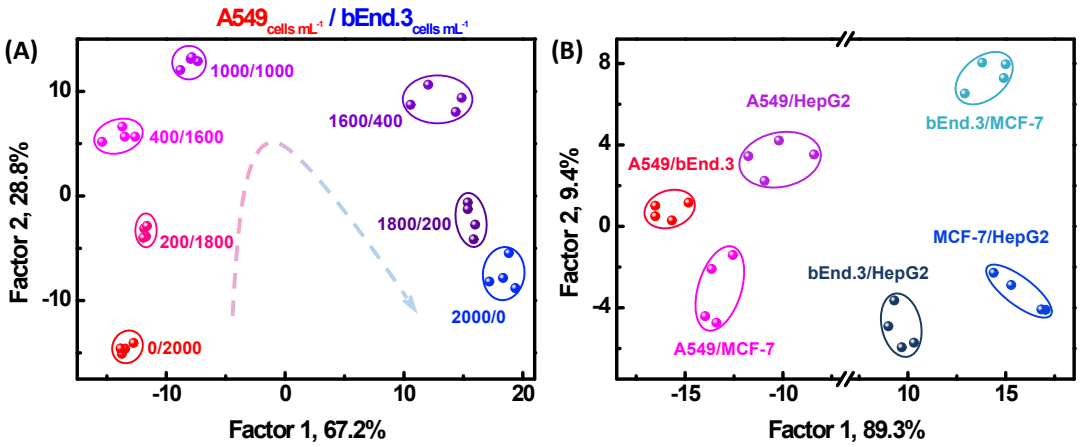

Fig. S10 LDA plot against (A) A549 and/or bEnd.3 cells (0/2000, 200/1800, 400/1600, 1000/1000, 1600/400, 1800/200, and 2000/0 cells mL^{-1}) and (B) A549/bEnd.3, A549/HepG2, A549/MCF-7, bEnd.3/HepG2, bEnd.3/MCF-7, and MCF-7/HepG2 cells (1000/1000 cells mL^{-1}). The total concentration was 2000 cells mL^{-1}.

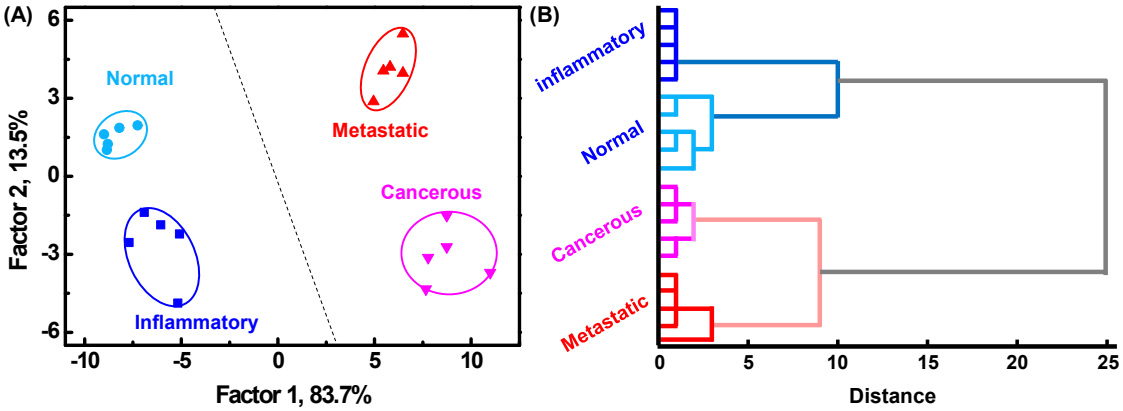

Fig. S11 (A) LDA plot and (B) HCA dendrogram of peripheral blood immunocyte samples from healthy, inflammatory, breast cancer, and metastatic breast cancer mice models at the concentration of 2000 cells mL^{-1}.

Table S1 FTIR spectra analysis of m-CPDs, o-CPDs, and p-CPDs.

Sample	Absorption peak (cm^{-1})	Group	Vibration mode
m-CPDs	~3400-3600	O-H	stretching vibration
	~3160-3400	N-H	stretching vibration
	1628	C=N	stretching vibration
	1450	C=C	stretching vibration
	1362	C-N=/NO_2	stretching vibration
	1173	C-H	in-plane bending vibration
	636/862	C-H	out-of-plane bending vibration
o-CPDs	~3400-3600	O-H	stretching vibration
	~3160-3400	N-H	stretching vibration
	1643	C=N	stretching vibration
	1500	C=C	stretching vibration
	1383	C-N=/-NO_2	stretching vibration
	1229	C-H	in-plane bending vibration
	750/833	C-H	out-of-plane bending vibration
p-CPDs	~3400-3600	O-H	stretching vibration
	~3160-3400	N-H	stretching vibration
	1630	C=N	stretching vibration
	1518	C=C	stretching vibration
	1393	C-N=/NO_2	stretching vibration
	1180	C-H	in-plane bending vibration

	841/756	C-H	out-of-plane bending vibration

Table S2 Fluorescence lifetime of m-CPDs, o-CPDs, and p-CPDs.

CPDs	T (ns)	χ^2
m-CPDs	6.99	0.995
o-CPDs	3.04	0.993
p-CPDs	5.43	0.997

Table S3 QY of m-CPDs, o-CPDs, and p-CPDs.

CPDs	QY (%)
m-CPDs	23.3
o-CPDs	14.6
p-CPDs	19.5

Table S4 Zeta potential of m-CPDs, o-CPDs, and p-CPDs.

CPDs	Zeta potential (mV)
m-CPDs	25.67
o-CPDs	3.58
p-CPDs	-9.2

Table S5 log*P* of m-CPDs, o-CPDs, and p-CPDs.

CPDs	**log*P***
m-CPDs	< 0.01
o-CPDs	2.21
p-CPDs	0.18

log*P* was determined according to Organization for Economic Co-operation and Development (OECD) Guidelines for the Testing of Chemicals-Partition coefficient (n-octanol/water): Shake flask method. m-CPDs is a hydrophilic product (log*P* < 0.01), which is not suitable for the determination of log*P* by the shake flask method.

Table S6 Yields of m-CPDs, o-CPDs, and p-CPDs.

CPDs	Yield (%)
m-CPDs	11.23
o-CPDs	10.38
p-CPDs	13.98

Table S7. Lines of cells used in this work.

Cell line	Origin	Cell status
MCF-7	breast	tumorigenic
MDA-MB-231	breast	metastatic
A549	lung	tumorigenic
K562	circulatory system	tumorigenic
HeLa	cervix	tumorigenic
HepG2	liver	tumorigenic
bEnd.3	mouse	non-tumorigenic

Table S8 Jackknifed classification matrix of LDA in cells discrimination.

CPDs			% Correct classification					
C 1	C 2	C 3	MCF-7	A549	bEnd.3	K562	HepG2	HeLa
			100	100	75	100	100	100
			100	100	50	100	75	0
			75	100	100	100	75	75
			100	100	100	100	100	100
			100	100	100	100	100	100
			100	100	100	100	100	100
			100	100	100	100	100	100

Table S9 Detection limits of this work and others.

Number	Detection Limit (cells mL^{-1})	Reference
1	2000	8
2	10000	9
3	1500	10
4	2000	11
5	10000	12
6	20000	13
7	1000	This work

Table S10 Fluorescent responses obtained from different concentrations of peripheral blood immunocytes from tumor-free and tumor-bearing mouse model using the sensor.

Samples	ID-cells mL^{-1}	Fluorescence Response Pattern		
		C 1	C 2	C 3
1	N-1000	-1.21107	-0.80275	-0.11725
2	N-1000	-1.45107	-0.73281	0.28543
3	N-1000	-2.13415	-0.54299	0.23806
4	N-1000	-1.37723	-0.75279	0.33281
5	N-1000	-1.19261	-1.09248	-0.89893
6	C-1000	-0.12185	1.08548	1.39873
7	C-1000	0.17354	1.16541	1.23292
8	C-1000	0.192	1.21536	1.30398
9	C-1000	0.09969	0.82573	1.46979
10	C-1000	-0.25108	1.25532	0.99605
11	N-2000	0.28431	-1.14243	-0.56731
12	N-2000	0.65354	-1.69191	-0.212
13	N-2000	-0.06646	-0.83272	0.59337
14	N-2000	0.30277	-0.65289	-0.56731
15	N-2000	0.85661	-1.09248	0.5223
16	C-2000	0.59815	0.57596	-0.54362
17	C-2000	1.61353	0.71583	-1.18318
18	C-2000	0.85661	0.70584	-1.18318
19	C-2000	1.11507	0.71583	-1.98854
20	C-2000	1.05969	1.07549	-1.11212

Table S11 Fluorescence responses obtained by the sensor from the peripheral blood immunocytes of five tumor-free and five tumor-bearing mice model at the concentration of 2000 cells mL^{-1}.

Samples	ID	Fluorescence Response Pattern		
		C 1	C 2	C 3
1	N-1	-0.58304	-0.17336	1.32014
2	N-1	-1.19019	-0.33069	0.85444
3	N-1	-1.16379	-0.36511	0.81161
4	N-1	-1.09339	-1.79092	0.81697
5	N-1	0.05051	-1.25009	1.27732
6	N-2	-0.84702	-1.33859	1.32014
7	N-2	-0.88221	-1.27468	1.18632
8	N-2	-1.19899	-1.609	0.41014
9	N-2	-1.31338	-1.20584	0.39408
10	N-2	-0.96141	-0.52735	0.34591
11	N-3	-0.85582	-0.56669	1.15956
12	N-3	-0.60944	-0.8666	1.28803
13	N-3	-1.0758	-0.78793	1.26661
14	N-3	-0.72383	0.03805	1.76979
15	N-3	-0.34546	-0.10453	1.70556
16	N-4	-1.0318	-0.34544	1.00967
17	N-4	-0.97021	-0.49294	0.8705
18	N-4	-1.18139	-1.98758	0.46903
19	N-4	-0.51264	-1.88433	0.3352
20	N-4	-0.62703	-0.57652	0.51185
21	N-5	-0.29266	-0.59127	0.46903
22	N-5	-0.21347	-0.65519	0.64032

23	N-5	-1.12859	-0.04061	1.26126
24	N-5	-0.26627	-0.26677	0.54932
25	N-5	-1.17259	-0.01111	1.06856
26	C-1	0.93923	-0.34544	-1.10474
27	C-1	0.92163	-0.29136	-1.08333
28	C-1	1.91595	-0.53719	-1.08333
29	C-1	1.24721	1.30162	-0.91204
30	C-1	0.84244	1.22295	-1.0298
31	C-2	1.15921	1.19837	-0.85851
32	C-2	0.58726	1.10987	-0.78892
33	C-2	1.60798	1.11479	-0.29109
34	C-2	0.86004	1.4737	-0.5748
35	C-2	2.4703	1.3557	-1.22786
36	C-3	1.79276	1.46387	-1.16362
37	C-3	0.78085	1.08529	-1.11009
38	C-3	1.00083	-0.31594	-1.08333
39	C-3	0.05931	0.84438	-0.88527
40	C-3	0.1913	0.24455	-0.85851
41	C-4	-0.61824	0.61821	-1.30815
42	C-4	0.1297	0.87879	-1.42592
43	C-4	-0.49505	1.3262	-1.37239
44	C-4	-0.46865	0.93287	-0.60156
45	C-4	0.65766	1.14429	-1.00304
46	C-5	1.03602	1.36553	-0.62298
47	C-5	0.99203	1.11479	-0.62298
48	C-5	0.64006	1.16395	-0.56409
49	C-5	0.94803	-0.17336	-0.77286
50	C-5	0.99203	-0.29136	-0.76215

Table S12 Identification of the blinded peripheral blood immunocytes from five tumor-free and five tumor-bearing mice model at the concentration of 2000 cells mL^{-1}.

Unknown samples	Fluorescence Response Pattern			Predicted as	Accuracy of identification
	C 1	C 2	C 3		
1	-1.09501	-0.24296	0.64804	N-1	Yes
2	-1.02047	-0.54818	0.53366	N-1	Yes
3	-0.79685	-0.46813	0.51732	N-1	Yes
4	-1.13228	0.37248	0.46829	N-1	Yes
5	-1.2534	0.22738	1.29622	N-1	Yes
6	-0.88071	0.15732	1.42694	N-2	Yes
7	-1.00183	-0.00279	1.40515	N-2	Yes
8	-0.62914	-0.03782	1.41605	N-2	Yes
9	-0.89003	-1.48886	1.45962	N-2	Yes
10	-1.11364	-0.93847	1.32345	N-2	Yes
11	-1.05774	-1.02853	1.91716	N-3	Yes
12	-0.14465	-0.96348	1.8518	N-3	Yes
13	-0.1726	-1.30373	1.1437	N-3	Yes
14	-0.08875	-0.89343	0.98575	N-3	Yes
15	-0.40553	-0.20294	0.94217	N-3	Yes
16	-0.52666	-0.26798	0.94762	N-4	Yes
17	-0.2285	-0.33303	1.39971	N-4	Yes
18	-0.95525	0.29242	0.67528	N-4	Yes
19	-0.7689	0.06226	1.20362	N-4	Yes
20	-0.50802	0.32244	0.63715	N-4	Yes
21	0.19077	-0.0178	0.59357	N-5	Yes
22	-0.75959	0.03724	0.76787	N-5	Yes

23	-0.48007	-0.21294	1.00209	N-5	Yes
24	-1.12296	1.65841	0.59357	N-5	Yes
25	-1.10432	1.57835	0.4574	N-5	Yes
26	0.83366	-0.0178	-1.21479	C-1	Yes
27	1.2343	-0.16791	-1.33462	C-1	Yes
28	-0.3869	-1.68901	-1.28015	C-1	Yes
29	-0.35895	-1.58393	-0.51759	C-1	Yes
30	-0.51734	-0.25297	-0.51759	C-1	Yes
31	0.27463	1.82353	-0.45767	C-2	Yes
32	0.20009	1.43825	-0.6701	C-2	Yes
33	0.33985	0.01222	-0.68644	C-2	Yes
34	0.9641	1.19307	-0.17988	C-2	Yes
35	1.19703	0.58263	-0.46857	C-2	Yes
36	2.75301	1.55333	-0.4958	C-3	Yes
37	2.03558	1.46327	-0.90431	C-3	Yes
38	1.83992	1.46827	-0.81172	C-3	Yes
39	1.04796	1.83353	-0.93155	C-3	Yes
40	1.36474	1.71345	-0.75725	C-3	Yes
41	0.75912	1.72345	-1.13308	C-4	Yes
42	1.45791	1.46827	-1.06772	C-4	Yes
43	1.02932	1.51831	-1.01325	C-4	Yes
44	1.11318	0.15732	-1.0078	C-4	Yes
45	2.16602	0.03724	-0.98602	C-4	Yes
46	2.03558	0.96291	-0.98602	C-5	Yes
47	1.13181	1.2281	-0.98602	C-5	Yes
48	1.18772	1.68343	-0.78448	C-5	Yes
49	0.81503	1.28314	-0.75725	C-5	Yes
50	1.14113	1.49829	-0.65921	C-5	Yes

References

1. (a) F. Obermeier, G. Kojouharoff, W. Hans, J. Scholmerich, V. Gross, W. Falk, *Clin. Exp. Immunol.* 1999, **116**, 238-245. (b) G. Kojouharoff, W. Hans, F. Obermeier, D. N. Mannel, T. Andus, J. Scholmerich, V. Gross, W. Falk, *Clin. Exp. Immunol.* 1997, **107**, 353-8. (c) J. Li, H. Chen, B. Wang, C. Cai, X. Yang, Z. Chai, We. Feng, *Sci. Rep.* 2017, **7**, 1-11.
2. (a) S. M. Shafie, L. A. Liotta, *Cancer Lett.* 1980, **11**, 81-87. (b) Z. Li, Y. Yu, M. Wang, H. Xu, B. Han, P. Jiang, H. Ma, Y. Li, C. Tian, D. Zhou, X. Li, X. Ye, *Sci. Rep.* 2019, **9**, 1-12. (c) X. Jiang, C. Cao, W. Sun, Z. Chen, X. Li, L. Nahar, S. D. Sarker, M. I. Georgiev, W. Bai, *Food. Chem. Toxicol.* 2019, **126**, 56-66.
3. (a) W. E. Hardman, G. Ion, *Nutr. Cancer* 2008, **60**, 666-674. (b) W. E. Hardman, C. J. Barnes, C. W. Knight, I. L. Cameron, *Br. J. Cancer* 1997, **76**, 347-354.
4. S. Rana, S. G. Elci, R. Mout, A. K. Singla, M. Yazdani, M. Bender, A. Bajaj, K. Saha, U. H. F. Bunz, F. R. Jirik, V. M. Rotello. *J. Am. Chem. Soc.* 2016, **138**, 4522-4529.
5. A. S. Glas, J. G. Lijmer, M. H. Prins, G. J. Bonsel, P. M. Bossuyt, *J. Clin. Epidemiol* 2003, **56**, 1129-1135.
6. D. Rodríguez-Padrón, A. D. Jodlowski, G. de Miguel, A. R. Puente-Santiago, A. M. Balu, R. Luque, *Green Chem.* 2018, **20**, 225-229.
7. J. Liu, D. Li, K. Zhang, M. Yang, H. Sun, B. Yang, *Small* 2018, **14**, 1703919.
8. Q. Liu, Y. C. Yeh, S. Rana, Y. Jiang, L. Guo, V. M. Rotello, *Cancer Lett.* 2013, **334**, 196-201.
9. S. Tomita, O. Niwa, R. Kurita, *Anal. Chem.* 2016, **88**, 9079-9086.

10. S. Rana, S. G. Elci, R. Mout, A. K. Singla, M. Yazdani, M. Bender, A. Bajaj, K. Saha, U. H. F. Bunz, F. R. Jirik, V. M. Rotello. *J. Am. Chem. Soc.* 2016, **138**, 4522-4529.
11. S. Tomita, S. Ishihara, R. Kurita, *ACS Appl. Mater. Interfaces* 2019, **11**, 6751-6758.
12. H. Sugai, S. Tomita, S. Ishihara, R. Kurita, *ACS Sens.* 2019, **4**, 827-831.
13. A. Bajaj, O. R. Miranda, I. B. Kim, R. L. Phillips, D. J. Jerry, U. H. F. Bunz, V. M. Rotello, *Proc. Natl. Acad. Sci. U. S. A.* 2009, **106**, 10912-10916.